Desalination and Water Treatment
www.deswater.com
doi: 10.5004/dwt.2021.27512

233 (2021) 311–318
September

Application of photo-Fenton dye removal with γ-Fe_2O_3/bentonite nanocomposites prepared by solid-state reaction in wastewater treatment

Nahid Hajipour, Mohammad Ghorbanpour*, Atabak Feizi

Faculty of Engineering, University of Mohaghegh Ardabili, Ardabil, Iran, email: Ghorbanpouruma.ac.ir

Received 18 February 2021; Accepted 11 June 2021

ABSTRACT

One of the important parameters in wastewater treatment is the removal of dye from it. As heterogeneous catalysts for photo-Fenton treatment of dye, iron oxide/bentonite nanocomposites are prepared by the solid-state reaction method at 300°C and 600°C. The catalysts are characterized by X-ray diffraction (XRD), Brunauer–Emmett–Teller (BET) surface area analysis, X-ray diffraction spectroscopy, scanning electron microscopy (SEM) and transmission electron microscopy (TEM). SEM, TEM, and XRD analysis show γ-Fe_2O_3 (hematite) particles that are formed and distributed on the bentonite. EDX results revealed the increased iron and decreased calcium and magnesium contents in FeB300 and FeB600 compared with the parent bentonite. The results indicate that the prepared nanocomposites have a lower BET surface area than the parent bentonite. XRD patterns of samples prove formation of γ-Fe_2O_3 particles. Finally, the degradation efficiency of MO reached 81% and 75% in the presence of FeB300 or FeB600 and H_2O_2 under irradiation within 90 min, respectively. Therefore, both prepared catalysts exhibit acceptable photo-Fenton catalytic activity.

Keywords: Iron oxide/bentonite nanocomposites; Photo-Fenton; Solid-state reaction

1. Introduction

In recent years, the rapid growth of industries has increased pollution from industrial wastewater entering the environment without treatment. One of the factors that are considered in wastewater treatment is the removal of dye. Due to the complex chemical structure and stability of dye pollutants used in various industries, they impose major environmental risks and prevent from light transmittance and poor biodegradability. Therefore, a wide range of chemical and physical treatment methods have been developed, such as adsorption, ion-exchange, photocatalysis and filtration [1]. Moreover, advanced oxidation processes have been also defined as promising alternatives based on the generation of highly reactive transitory species (OH, O_2) for destruction of organic pollutants [2,3]. The Fenton reaction as a fast and economic method has attracted a huge deal of attention among the advanced oxidation processes as a result of reaction's strong oxidative capacity for the degradation of organic contaminants [4–6]. These processes generate highly reactive hydroxyl radicals using reagents such as Fe^{2+} and H_2O_2 under light irradiation as follows:

$$H_2O_2 + Fe^{2+} \rightarrow Fe^{3+} + OH^{\bullet} + OH^- \quad (1)$$

Following a chain reaction:

$$Fe^{3+} + H_2O_2 \rightarrow Fe^{2+} + HO_2^{\bullet} + H^+ \quad (2)$$

$$OH^{\bullet} + H_2O_2 \rightarrow HO_2^{\bullet} + H_2O \quad (3)$$

$$OH^{\bullet} + Fe^{2+} \rightarrow Fe^{3+} + OH^- \quad (4)$$

$$Fe^{3+} + HO_2^{\bullet} \rightarrow Fe^{2+} + O_2 + H^+ \quad (5)$$

* Corresponding author.

$$Fe^{2+} + HO_2^{\bullet} + H^+ \rightarrow Fe^{3+} + H_2O_2 \quad (6)$$

$$HO_2^{\bullet} + HO_2^{\bullet} \rightarrow H_2O_2 + O_2 \quad (7)$$

$$HO_2^{\bullet} + H_2O_2 \rightarrow OH^{\bullet} + H_2O + O_2 \quad (8)$$

The reaction between H_2O_2 and Fe^{3+} (reaction (2)), referred to as Fenton-like reaction, produces less oxidant radical species ($HO_2^{\bullet}$). The homogeneous catalytic decomposition of H_2O_2 by ferric ions may be also represented by:

$$Fe^{3+} + H_2O_2 \leftrightarrow Fe(HO_2)^{2+} + H^+ \quad (9)$$

$$Fe(HO_2)^{2+} \leftrightarrow Fe^{2+} + HO_2^{\bullet} \quad (10)$$

The photo-Fenton process increases the amount of $OH^{\bullet}$ radicals with Fe^{2+} regeneration (reaction (12)) by the photoreduction of $Fe(HO)^{2+}$, produced in reaction (11):

$$Fe^{3+} + H_2O \rightarrow Fe(HO)^{2+} + H^+ \quad (11)$$

$$Fe(HO)^{2+} + h\nu\ (\lambda < 400\ nm) \rightarrow Fe^{2+} + OH^{\bullet} \quad (12)$$

Thus, solar light irradiation (UV/visible irradiation) promotes photochemical reactions with light active intermediate species, such as $Fe(HO)^{2+}$. Through reaction (12), hydroxyl radicals and regenerates Fe^{2+} are produced closing the catalytic cycle of $OH^{\bullet}$ generation via the reaction (Eq. 1) [4,5,7].

Interestingly, iron oxide nanoparticles could also serve as Fenton reagent [6,7]. The photocatalytic activity of iron oxide nanoparticles arises from their semiconductor properties. These oxides have a low cost, low toxicity, biocompatibility, excellent chemical stability and ease of production [8]. They also absorb most visible light. Among different iron oxide nanoparticles, γ-Fe_2O_3 absorbs light up to 600 nm and collects up to 40% of solar spectrum energy. It also is one of the cheapest semiconductor materials [9].

Unfortunately, homogeneous photo-Fenton processes require high Fe concentration. Recovery of the consumed Fe ions from the produced sludge is expensive and time-consuming [6]. To overcome this drawback, Fe catalysts immobilization is applied to a suitable substrate [10]. In this area, porous substrates such as zeolites, clays, polymers, silica, and carbon are promising [11–15]. Among these substrates, clays are considered as good candidates due to their unique characteristics such as high surface area, abundant, low cost, and high porosity [16,17].

Bentonite is classified in montmorillonite clays with layered silicates. These layers include an alumina octahedral sheet, which is sandwiched between two silica tetrahedral sheets. Such layers are stacked by weak dipolar or van der Waals forces, leading to the interaction of charge compensating cations into the interlayer space. Therefore, not only adsorption on the external surface but also intercalation into the interlayer space can occur. Therefore, intercalation into the interlayer space can occur [18]. The intercalation of iron into the interlayer space of bentonite is achieved by the solid-state ion-exchange method [6,10]. Accordingly, bentonite is mixed with proper amounts of salt and heated by a furnace at a temperature close to the melting point of the salt. The reaction displaces calcium ions present in bentonite interlayers by Fe ions present in the molten salt of iron chloride [6,10,13,14]. The chemical reaction is represented as follows:

$$FeCl_2 + FeCl_3 + \text{bentonite: } Ca^{2+} \Rightarrow \text{bentonite: } Fe^{2+} + CaCl_2 \quad (13)$$

Moreover, heating in the air atmosphere oxidizes the exchanged Fe^{2+} ions into Fe_xO_y particles.

$$\text{Bentonite: } Fe^{2+} + O_2 \Rightarrow \text{bentonite: } Fe_xO_y \quad (14)$$

Furthermore, Karami [19] proposed a simple solid-phase method to synthesize γ-Fe_2O_3 nanoparticles.

In this method, iron oxide nanoparticles are prepared by the precipitation of Fe^{2+} or Fe^{3+} in liquid molten salts by adding a suitable base as a reducing agent. The reaction of iron chloride and potassium hydroxide as reducing agents forms iron oxide particles as follows:

$$FeCl_2 + 2FeCl_3 + 8\ KOH \Rightarrow 8\ KCl + Fe_3O_4 + 4\ H_2O \quad (15)$$

$$4Fe_3O_4 + O_2 \Rightarrow 6\gamma\text{-}Fe_2O_3 \quad (16)$$

The surface of bentonite contributes to the nucleation of nanoparticles during the reduction process [20]. The produced KCl salt and water molecules as the by-products help to produce smaller size particles and prevent their growth [19].

Therefore, it appears that by adding a suitable reducing agent to the mixture during solid ion exchange, in addition to intercalation of iron into the interlayer space of bentonite, iron nanoparticles are formed on its surface.

According to previous studies, the solid-state ion-exchanged clays showed acceptable antibacterial, adsorption, and photocatalytic activities [13,14,16,17]. For example, the use of copper-ion exchanged bentonite in the chitosan biopolymer film improved the film's antimicrobial and mechanical properties [21]. Besides, the solid-state iron-exchanged bentonite had a higher efficiency in dye removal of edible oil and dye absorption from the solution compared with bentonite [22]. Wang et al. [23] reported that the formation of Fe_2O_3–Fe_3O_4 nanocomposites supported by montmorillonite increased the degradation rate of methyl orange by a 1.61-fold, compared with pure Fe_2O_3–Fe_3O_4. Khoroshi and Ghorbanpour [6] studied methylene blue photo-Fenton degradation using solid-state ion exchanged bentonite with iron. In another study, rhodamine b was degraded in the presence of hydrogen peroxide and a catalyst. Although the type of dye was different from the present work, the dye concentration in their study was much lower and the amount of catalyst was higher [24]. Another study addressed the dye removal of iron-pillared bentonite vs. azo dye X-3B [22].

In the present work, a reductant is added to the mixture of molten salt and bentonite before heating. In this case, in addition to the solid-phase ion exchange, due to the presence of a reducing agent in the molten salt, the iron reduction and nanoparticles' synthesis are expected to occur in

the solid phase. The dye removal ability of the prepared composites in the photo-Fenton reaction is also investigated.

2. Experiment

$FeCl_2{\cdot}4H_2O$, $FeCl_3{\cdot}6H_2O$, KOH, methyl orange (MO), H_2O_2, and other reagents are purchased from Merck Company (Germany) and used without further purification.

2.1. Preparation of nanocomposites

For the synthesis of iron oxide/bentonite nanocomposites, $FeCl_3{\cdot}6H_2O$ (1.35 g), $FeCl_2{\cdot}4H_2O$ (0.50 g), KCl (3.9 g), and bentonite (3 g) powders are mixed and grounded to obtain a yellow paste. Then, some KOH powder (1.12 g) is added to this mixture and grounded for another 30 min. These two steps are carried out at room temperature. Then, the mixture is heated at 300°C and 600°C for 1 h. The obtained product is adequately washed with distilled water and filtered several times until no chloride ion is observed. Finally, the product is dried at 50°C for 3 h [4]. For simplicity, bentonite and the prepared composites in 300°C and 600°C are named Be, FeB300, and FeB600, respectively.

2.2. Characterization

Scanning electron microscopy (SEM) and elemental dispersive X-ray spectroscopy (EDX) are carried out with an LEO 1430VP instrument. A transmission electron microscope (Philips CM120, Germany) is used to analyze the morphology of the prepared composites. The X-ray diffraction (XRD) patterns of the samples are characterized using an X-ray diffractometer (Philips PW 1050, The Netherlands) with CuKα radiation (λ = 1.5418 Å, 40 kV and 30 mA, 2 θ from 0 to 80° and 0.05° step). BET analyzer (Gemini 2375, Germany) is used to evaluate the porosity of the prepared composite.

2.3. Photo-Fenton activity

The photo-Fenton tests are carried out using a Pyrex open vessel (250 mL) containing 100 mL of the aqueous solution of MO (pH = 4, 150 ppm). This container is placed on a magnetic stirrer and irradiate with a UV lamp (UVC, 4 W, Philips). The distance between the surface of the solution and the UV source is kept constant at 15 cm, in all experiments. The prepared nanocomposites (0.0792 g) and H_2O_2 (30 mM) are added to the reaction vessel. The moment of adding H_2O_2 is considered as the reaction initiation. During the reaction, the liquid aliquots are retrieved from the vessel at the selected periods and centrifuged. The dye removal efficiency is estimated as follows:

$$\text{Dye removal efficiency} = \left[\frac{C_0 - C_t}{C_t}\right] \times 100\% \tag{17}$$

where C_0 and C_t (mg L^{-1}) are the liquid-phase concentration of MO at the initial and subsequent time t, respectively, which is measured by spectrophotometer.

3. Results and discussion

3.1. Characterizations

A typical configuration of the bentonite with a sheet-like structure and large flakes is observed in Fig. 1a. Accordingly, some differences are imposed in the morphology of bentonite after the formation of nanocomposite (Figs. 1b and c). This difference arises from the loading and pillaring of iron oxide nanoparticles dispersed on the surface of the clay. Thus, the modified bentonite shows some irregular small particles distributed in the bentonite layer, which is the result of the formation of nanoparticles in the process of the co-precipitation process.

Fig. 2 shows the TEM images of FeB300 and FeB600. In this image, the dark- granules are iron oxide nanoparticles present in the interlayer space or on the bentonite surface. According to a previous report, due to the high density of ion-exchange sites on bentonite, the highly charged iron oxide nanoparticles are strongly bounded by the electrostatic interaction on the surface [19].

It should be noted that the SEM images show the formed nanoparticles on the surface of bentonite during the co-precipitation reaction. On the other hand, the ion exchange process occurs simultaneously, which forms particles between the bentonite interlayers (Fig. 2).

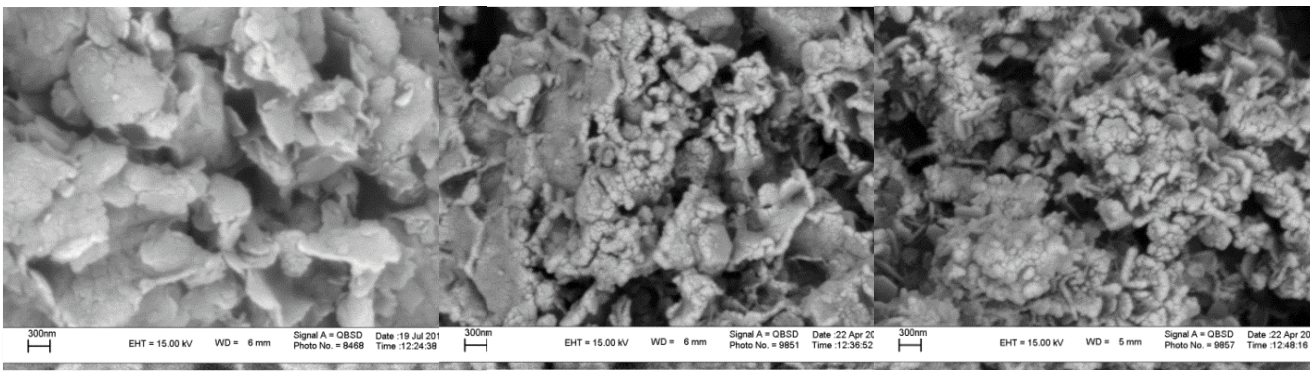

(a) (b) (c)

Fig. 1. Scanning electron microscopy images of parent bentonite (a), FeB300 (b) and FeB600 (c).

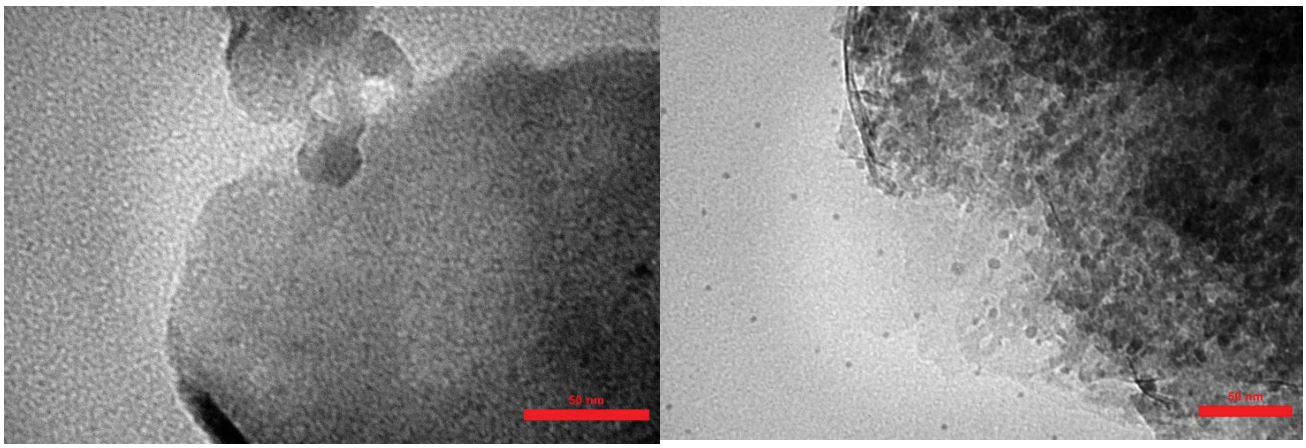

Fig. 2. Transmission electron microscopy images of FeB300 (a) and FeB600 (b).

The chemical composition of parent bentonite, FeB300 and FeB600 is shown in Fig. 3. The obtained results are summarized in Table 1. The results indicated increased iron and decreased calcium and magnesium contents in FeB300 and FeB600 compared with parent bentonite. Meanwhile, the Ca^{2+} and Mg^{2+} in bentonite interlayer are exchanged by the Fe ions, which confirm the formation of oxide/bentonite nanocomposites. Additionally, this table confirms the presence of elemental compounds of bentonite and iron oxide in the prepared composite without any impurity. The results indicate that the synthesized composite is highly pure.

According to the results of EDX analysis, the amount of iron in the sample FeB600 is about 29wt% and that of the sample FeB300 is about 17wt%. SEM images confirm this result as well. At higher temperatures, the rate of co-precipitation reaction is higher; therefore, more iron particles are formed on the surface. The amount of iron deposited in the present study is several times higher than the previous works in which ion exchange was applied to prepare iron oxide/bentonite composite [6,10]. The reason is the limited ion exchange capacity of bentonite, which has a low capacity and does not allow further increase in iron content in the composite after saturation. In the present study, nanoparticles are formed on the surface in addition to the interlayer space. Therefore, a larger content is present in the composite.

Fig. 4 reveals X-ray diffraction patterns of bentonite, FeB300 and FeB600. A typical reflection of bentonite is observed at $2\theta = 6.28°$ (d = 1.40 nm) corresponding to the (001) reflection of bentonite structure. Other reflections corresponding to montmorillonite's crystalline structure at 19.84° and 26.68° can be indexed to (110) and (210) planes of the bentonite, respectively [6,8].

These peaks appear in the patterns of all nanocomposites. However, after ion exchange, due to the loss of water initially present in the interlayers, the original d spacing in the montmorillonite clay decreased to 1.21 nm for FeB300 and disappeared for FeB600 [10]. Furthermore, this indicates a high disorder of the structure of parent bentonite, which is referred to as "delaminated clay". In other words, the highly ordered parallel lamellar structure of the montmorillonite's crystalline structure is disrupted by the formation of the Fe_3O_4 nanoparticles.

On the other hand, comparing FeB300 and FeB600 with bentonite, new peaks appeared at 2θ values of 30.27°, 35.68°, 43.0, 57.40° and 63.01° corresponding to the lattice planes of (222), (400), (332), (530) and (532) from the cubic structure of γ-Fe_2O_3 [9,19].

This proves that γ-Fe_2O_3 is successfully formed under preparation condition. Accordingly, the iron ions penetrated the interlayer space of montmorillonite via the ion exchange. They were reduced by NaOH to Fe_3O_4 nanoparticles on the bentonite surface. In the case of exchanged iron, the interlayer space would act as a size controller.

The nitrogen adsorption–desorption isotherms and the pore size distribution curves of parent bentonite, FeB300 and FeB600 are demonstrated in Fig. 5. The corresponding parameters of samples including BET surface area, total pore volume and average pore size were summarized in Table 2. The isotherms showed that parent bentonite, FeB300 and FeB600 present a typical type IV pattern, indicating the presence of mesoporous structure in the size range of 2–50 nm. The hysteresis loops of these isotherms were of H3 type, indicating that narrow slit-shaped pores are associated with plate-like particles [25]. According to Table 2, the parent bentonite has the highest surface area. The formation of nanoparticles and intercalation during pillarization lead to the surface area decreasing owing to partial blocking of the bentonite pores by surface and pillared nanoparticles [2]. Furthermore, as discussed earlier, the loss of water existing initially in the interlayers of bentonite reduced its basal spacing.

3.2. Photo-Fenton activity

The catalytic degradation efficiencies of MO by FeB300 and FeB600 are analyzed under different experimental conditions (Fig. 6). The photo-Fenton activity demonstrated that MO could not be oxidized in the presence of H_2O_2, composite, or UV, alone. The removal of MO caused by H_2O_2 and UV is negligible (<5%) compared with the one caused

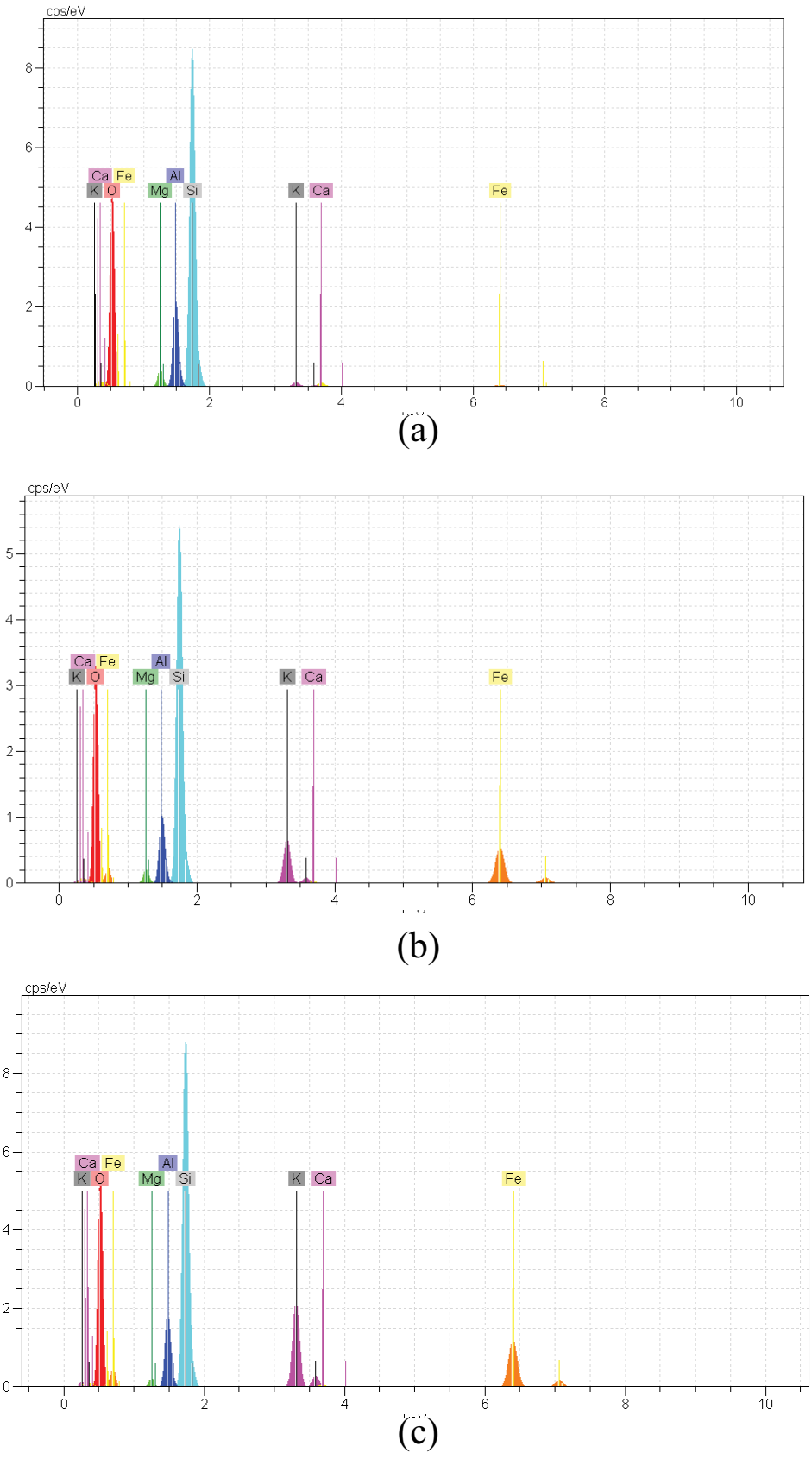

Fig. 3. Energy dispersive X-ray spectroscopy of parent bentonite (a), FeB300 (b) and FeB600 (c).

by the oxidation process in the later experiments [27]. With the catalyst in the dark and without H_2O_2, due to the adsorption of dye by catalysts, the degradation efficiency of MO increased to about 16% and 13% for FeB300 and FeB600, respectively. Higher degradation, that is 29.0% or 25.4%, is achieved in the presence of FeB300 and FeB600 under irradiation because UV irradiation improves the degradation of organic pollutants by photolysis of iron species. H_2O_2 in the presence of FeB300 and FeB600 results in a heterogeneous Fenton-like system with 67% or 59% degradation. In this system, Fe^{2+} catalyzed decomposition of H_2O_2 is the driving force for the formation of hydroxyl radicals. This reaction happens at a relatively low rate and the oxidation of MO by hydroxyl radical could not proceed effectively.

Table 1
Chemical composition of the parent bentonite, FeB300 and FeB600

	Be	FeB300	FeB600
Oxygen	55.19	45.76	36.78
Magnesium	1.58	1.11	0.63
Aluminium	8.10	5.53	6.21
Silicon	31.55	29.74	26.74
Potassium	0.79	0.74	0.31
Calcium	0.61	0.08	0.03
Iron	0.92	17.05	29.28

Table 2
Surface area, average pore radius and total pore volume of samples

	Be	FeB300	FeB600
V_p ($cm^3 g^{-1}$)	0.1142	0.0487	0.0187
r_p (nm)	1.66	1.66	1.22
a_p ($m^2 g^{-1}$)	85.04	31.53	8.86

The degradation efficiency of MO reached 81% or 75% in the presence of FeB300 or FeB600 and H_2O_2 under irradiation within 90 min, respectively. In this system, Fe^{3+} is converted to Fe^{2+} by photo-reduction on the surface of the catalyst. Then, the formed Fe^{2+} reacts with H_2O_2 to produce hydroxyl radicals, while it is oxidized by H_2O_2 to form Fe^{3+} to form the Fe^{3+}/Fe^{2+} cycle. At last, the generated hydroxyl radicals attack the MO molecules, the dye molecules are degraded to CO_2, and H_2O and the catalyst is restored to the original state.

As mentioned previously, FeB300 slightly outperformed FeB600 in terms of the degradation efficiency of MO. This result is associated with the smaller size of the formed nanoparticles and higher specific surface area, which offers more active sites. As a result, the composite prepared at a lower temperature is preferred to show the best photodegradation performance. Using solid ion exchanged bentonite with iron, Khoroshi and Ghorbanpour [6] provided full dye removal of methylene blue solution (200 ppm) in the presence of hydrogen peroxide (30 mM) and catalyst (0.4 g/L) during 90 min at pH = 4. In present study, methyl orange solution (150 ppm) provided 80% efficiency in the presence of a much smaller amount of catalyst (0.0792 g). In another study, the dye

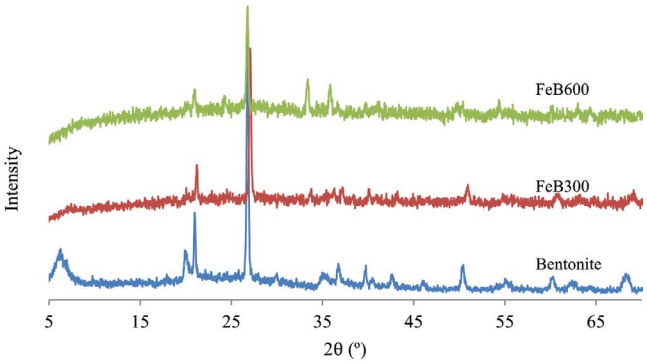

Fig. 4. X-ray diffraction patterns of bentonite, FeB300 and FeB600.

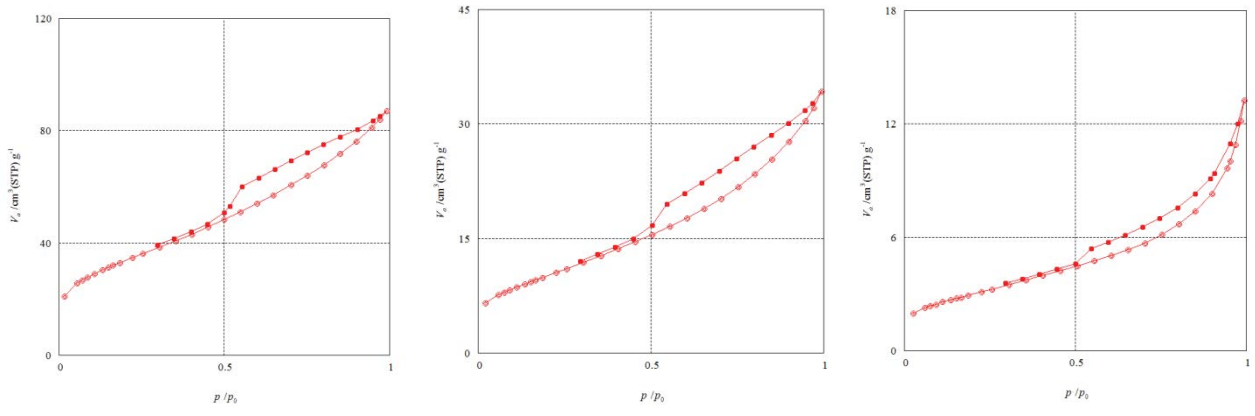

Fig. 5. N_2 adsorption–desorption isotherms of parent bentonite (a), FeB300 (b) and FeB600.

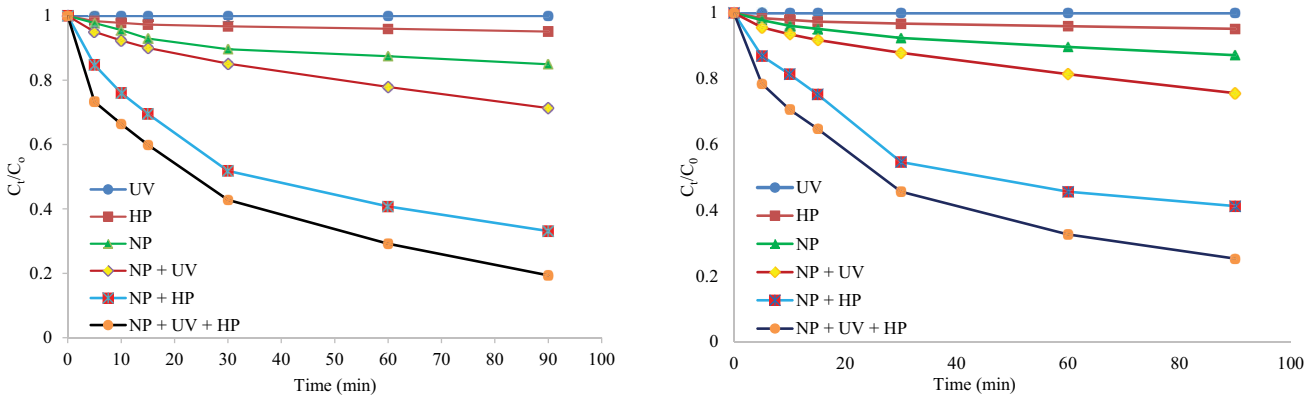

Fig. 6. Decolonization of MO (150 ppm, 0.0792 g catalyst, 30 mM H_2O_2 and pH = 4) by FeB300 (a) and FeB600 (b).

solution (rhodamine b) (20 ppm) was completely removed in the presence of hydrogen peroxide (10 mM) and a catalyst (0.2 g/L) at pH = 4.25 within 30 min. Although the type of dye was different from the present work, their dye concentration was much lower and the amount of catalyst was higher [25]. Another study addressed the dye removal of iron-pillared bentonite vs. Azo dye X-3B. Compared with the present laboratory work, they achieved 100% removal at a lower concentration and a higher amount of adsorbent (approximately six times greater) at a lower pH. Besides, their synthesis took about 4 days, which is only few hours and much easier in the present study [26].

4. Conclusion

The present work investigated the photo-Fenton dye removal ability of the γ-Fe_2O_3 /bentonite nanocomposites prepared by solid state at 300°C and 600°C. Characterization of the prepared nanocomposite demonstrated γ-Fe_2O_3 (hematite) particles, which are formed and distributed on the bentonite. EDX results revealed increased iron and decreased calcium and magnesium contents in FeB300 and FeB600 compared with the parent bentonite. The results indicate that the prepared nanocomposites have a lower BET surface area than the parent bentonite. Finally, the degradation efficiency of MO reached 81% or 75% in the presence of FeB300 or FeB600 and H_2O_2 under irradiation within 90 min, respectively. Therefore, both prepared catalysts exhibit acceptable photo-Fenton catalytic activity.

References

[1] G. Fadillah, S.P. Yudha, S. Sagadevan, I. Fatimah, O. Muraza, Magnetic iron oxide/clay nanocomposites for adsorption and catalytic oxidation in water treatment applications, Open Chem., 18 (2020) 1148–1166.
[2] M. Ghorbanpour, A. Feizi, Application of synthesizing trimetallic Zn and Ag co-doped TiO_2 nano-photocatalyst by a one-step synthesis technique in treating water pollutants, Desal. Wat. Treat., 200 (2020) 187–195.
[3] M. Madadi, M. Ghorbanpour, A. Feizi, Preparation and characterization of solar light-induced rutile Cu-doped TiO_2 photocatalyst by solid-state molten salt method, Desal. Wat. Treat., 145 (2019) 257–261.
[4] A. Babuponnusami, K. Muthukumar, A review on Fenton and improvements to the Fenton process for wastewater treatment, J. Environ. Chem. Eng., 2 (2014) 557–572.
[5] N. Wang, T. Zheng, G. Zhang, P. Wang, A review on Fenton-like processes for organic wastewater treatment, J. Environ. Chem. Eng., 4 (2016) 762–787.
[6] S.K. Khoroshi, M. Ghorbanpour, Catalytic activity of Fe-modified bentonite in heterogeneous photo-Fenton process, Desal. Wat. Treat., 162 (2019) 376–382.
[7] G. Gutierrez-Mata, S. Velazquez-Martínez, A. Álvarez-Gallegos, M. Ahmadi, J. Alfredo Hernández-Pérez, F. Ghanbari, S. Silva-Martínez, Recent overview of solar photocatalysis and solar photo-Fenton processes for wastewater treatment, Int. J. Photoenergy, 2017 (2017) 8528063, doi: 10.1155/2017/8528063.
[8] S.A. Ziabari, M. Babamoradi, Z. Hajizadeh, A. Maleki, The effect of magnetic field on the magnetic and hyperthermia properties of bentonite/Fe_3O_4 nanocomposite, Phys. B, 588 (2020) 412167.
[9] M. Saad, H. Tahir, Synthesis of carbon loaded γ-Fe_2O_3 nanocomposite and their applicability for the selective removal of binary mixture of dyes by ultrasonic adsorption based on response surface methodology, Ultrason. Sonochem., 36 (2017) 393–408.
[10] R. Shayegh, M. Ghorbanpour, A new approach for the preparation of iron oxide-pillared bentonite as adsorbent of dye, Desal. Wat. Treat., 183 (2020) 404–412.
[11] S. Lotfiman, M. Ghorbanpour, Antimicrobial activity of ZnO/silica gel nanocomposites prepared by a simple and fast solid-state method, Surf. Coat. Technol., 310 (2017) 129–133.
[12] M. Ghorbanpour, B. Hakimi, A. Feizi, A comparative study of photocatalytic activity of ZnO/activated carbon nanocomposites prepared by solid-state and conventional precipitation methods, J. Nanostruct., 8 (2018) 259–265.
[13] M. Ghorbanpour, S. Lotfiman, Solid-state immobilisation of titanium dioxide nanoparticles onto nanoclay, Micro Nano Lett., 11 (2016) 684–687.
[14] H. Pouraboulghasem, M. Ghorbanpour, R. Shayegh, S. Lotfiman, Synthesis, characterization and antimicrobial activity of alkaline ion-exchanged ZnO/bentonite nanocomposites, J. Cent. South Univ., 23 (2016) 787–792.
[15] Q.L. Zhu, Q. Xu, Immobilization of ultrafine metal nanoparticles to high-surface-area materials and their catalytic applications, Chem, 1 (2016) 220–245.
[16] M. Ghorbanpour, M. Mazloumi, A. Nouri, S. Lotfiman, Silver-doped nanoclay with antibacterial activity, J. Ultrafine Grained Nanostruct. Mater., 50 (2017) 124–131.
[17] H. Pourabolghasem, M. Ghorbanpour, R. Shayegh, Antibacterial activity of copper-doped montmorillonite nanocomposites prepared by alkaline ion exchange method, J. Phys. Sci., 27 (2016) 1–12.

[18] M.H. Latif, F.L. Yahya, Preparation and characterization of new magnetic montmorillonite clay mineral by intercalation of iron oxides in West Iraqi layered bentonite, Chem. Mater. Res., 7 (2015) 55–62.
[19] H. Karami, Synthesis and characterization of iron oxide nanoparticles by solid state chemical reaction method, J. Clust. Sci., 21 (2010) 11–20.
[20] K. Kalantari, M.B. Ahmad, K. Shameli, M.Z.B. Hussein, R. Khandanlou, H. Khanehzaei, Size-controlled synthesis of Fe_3O_4 magnetic nanoparticles in the layers of montmorillonite, J. Nanomater., (2014) 1–9.
[21] A. Nouri, M.T. Yaraki, M. Ghorbanpour, S. Agarwal, V.K. Gupta, Enhanced antibacterial effect of chitosan film using montmorillonite/CuO nanocomposite, Int. J. Biol. Macromol., 109 (2018) 1219–1231.
[22] M. Ghorbanpour, Soybean oil bleaching by adsorption onto bentonite/iron oxide nanocomposites, J. Phys. Sci., 29 (2018) 113–119.
[23] J. Wang, Y. Chen, G. Liu, Y. Cao, Synthesis, characterization and photocatalytic activity of inexpensive and non-toxic Fe_2O_3– Fe_3O_4 nano-composites supported by montmorillonite and modified by grapheme, Compos. Part B, 114 (2017) 211–22.
[24] S. Pandey, A comprehensive review on recent developments in bentonite-based materials used as adsorbents for wastewater treatment, J. Mol. Liq., 241 (2017) 1091–1113.
[25] S. Chen, Y. Wu, G. Li, J. Wu, G. Meng, X. Guo, Z. Liu, A novel strategy for preparation of an effective and stable heterogeneous photo-Fenton catalyst for the degradation of dye, Appl. Clay Sci., 136 (2017) 103–111.
[26] Y. PLi, Y. Lu, X. Zhu, Photo-Fenton discoloration of the azo dye X-3B over pillared bentonites containing iron, J. Hazard. Mater., 132 (2006) 196–201.